How to cite: *Angew. Chem. Int. Ed.* **2024**, *63*, e202319162
doi.org/10.1002/anie.202319162

Coordination Polymers

On-Surface Isomerization of Indigo within 1D Coordination Polymers

Hongxiang Xu, Ritam Chakraborty, Abhishek Kumar Adak, Arpan Das, Biao Yang, Dennis Meier, Alexander Riss, Joachim Reichert,* Shobhana Narasimhan,* Johannes V. Barth,* and Anthoula C. Papageorgiou**

Abstract: Natural products are attractive components to tailor environmentally friendly advanced new materials. We present surface-confined metallosupramolecular engineering of coordination polymers using natural dyes as molecular building blocks: indigo and the related Tyrian purple. Both building blocks yield identical, well-defined coordination polymers composed of (1 dehydroindigo : 1 Fe) repeat units on two different silver single crystal surfaces. These polymers are characterized atomically by submolecular resolution scanning tunnelling microscopy, bond-resolving atomic force microscopy and X-ray photoelectron spectroscopy. On Ag(100) and on Ag(111), the *trans* configuration of dehydroindigo results in N,O-chelation in the polymer chains. On the more inert Ag(111) surface, the molecules additionally undergo thermally induced isomerization from the *trans* to the *cis* configuration and afford N,N- plus O,O-chelation. Density functional theory calculations confirm that the coordination polymers of the *cis*-isomers on Ag(111) and of the *trans*-isomers on Ag(100) are energetically favoured. Our results demonstrate post-synthetic linker isomerization in interfacial metal-organic nanosystems.

Introduction

Indigo (molecular reactant in top row of Scheme 1) is a common, ancient pigment with a distinctive blue colour. More recently, its molecular properties have attracted wide interest.[1] Among them, the various metal complexes of indigo[2] and its derivatives[3] have been explored and found application in redox-[4] and electro-[5] chemistry as redox-switchable ionophores[6] and organic-based battery materials.[5] Notably, indigo can chelate metal ions with its N and O atoms. Thus, individual metal complexes sandwiched between two indigo derivatives have been created and studied on surfaces.[7] Extension of this coordination offers the possibility of forming natural compound coordination polymers (CPs), such as the Ni–CPs of the related natural dye, Tyrian purple (6,6′-dibromoindigo, molecular reactant in bottom scheme 1).[8] CPs exhibit desirable properties for gas adsorption and packing,[9] catalysis[10] and photoluminescence.[11] More recently, surface-confined metallosupramolecular engineering has emerged as a route towards unique CPs[13] with unconventional electronic[14] and magnetic properties,[15] making them suitable for multiple applications including magnetic information storage and spintronics.[12]

The isomerization of indigo is an interesting challenge, both as basic research topic and for its practical applications. It provides a handle to switch the molecular functionalities which is expected to have a strong impact on the electronic and optical properties. The neutral indigo has an intriguingly high photostability[16] and its *trans-cis* photoisomerization has been the subject of scrutiny for mechanistic insights.[17] The factors inhibiting photoisomerization in indigo include intramolecular NH···O=C hydrogen bonds in the *trans* isomer, efficient excited-state proton transfer, and efficient nonradiative internal conversion.[17a,18] Interestingly, in the absence of the intramolecular H-bonds, *N,N′*-disubstituted

[*] H. Xu, Dr. B. Yang, D. Meier, Dr. A. Riss, Dr. J. Reichert, Prof. J. V. Barth, Dr. A. C. Papageorgiou
Technical University of Munich, TUM School of Natural Sciences, Physics Department E20
James Franck Strasse 1, 85748 Garching (Germany)
E-mail: joachim.reichert@tum.de
jvb@tum.de

R. Chakraborty, Dr. A. K. Adak, A. Das, Prof. S. Narasimhan
Theoretical Sciences Unit & School of Advanced Materials, Jawaharlal Nehru Centre for Advanced Scientific Research
Jakkur, Bangalore 560054 (India)
E-mail: shobhana@jncasr.ac.in

Dr. A. K. Adak
Current address: The Abdus Salam International Centre for Theoretical Physics
Strada Costiera 11, 34151 Trieste (Italy)

Dr. B. Yang
Institute of Functional Nano and Soft Materials (FUNSOM), Jiangsu Key Laboratory for Carbon-Based Functional Materials and Devices, Soochow University
Suzhou, 215123 (P. R. China)
E-mail: yangbiao@suda.edu.cn

Dr. A. C. Papageorgiou
Laboratory of Physical Chemistry, Department of Chemistry, National and Kapodistrian University of Athens
Panepistimiopolis, 15771 Athens (Greece)
E-mail: a.c.papageorgiou@chem.uoa.gr

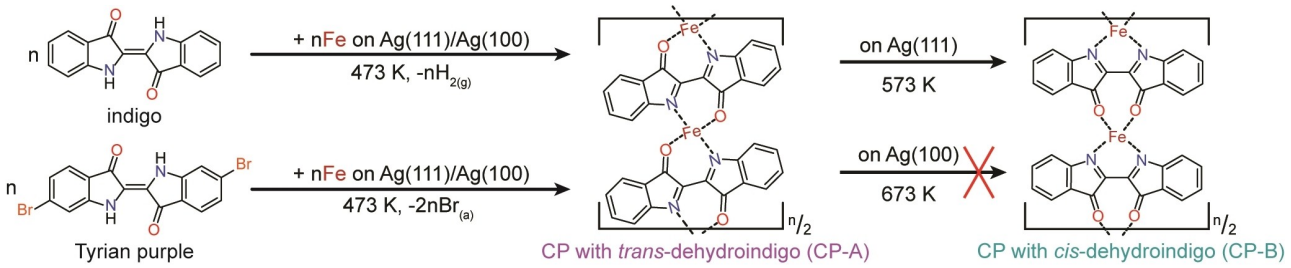

Scheme 1. On-surface formation of CPs presented in this work. *Trans* and *cis* molecular monomers of dehydroindigo afford N,O– and N,N– plus O,O-chelation within the CPs.

indigos[19] (such as *N,N′*-diacyl,[20] *N,N′*-dimethyl,[17b,21] and *N,N′*-di(tert-butyloxycarbonyl)[22] indigos) undergo photoisomerization, expanding their application in photoswitches.[23] In addition, isomerization of indigo can be induced by heating,[24] protonation[25] and catalysts such as transition metal ions.[2a,d] In particular, *cis*-indigo is posited as a promising material for optoelectronic devices, based on calculated electronic properties by density functional theory (DFT).[26]

Here we explore surface confined nanostructuring, providing access to otherwise unattainable compounds. This approach is conveniently coupled with direct visualization and molecular identification using scanning probe microscopy techniques such as scanning tunnelling microscopy (STM) and noncontact atomic force microscopy (nc-AFM) with CO-functionalized tips.[27] In particular one-dimensional (1D) CPs[14a,15a,28] have been fabricated and isolated through careful development of interfacial metallosupramolecular engineering protocols,[29] relying on metal-ligand interactions operative between metal adatoms and suitable linker groups. Specifically, we observe metal-directed assembly of distinct 1D CPs incorporating dehydroindigo molecules and iron adatoms on the Ag(111) and Ag(100) surfaces. Combining analysis of STM, AFM and X-ray photoelectron spectroscopy (XPS) measurements with DFT calculations, we identified the *trans* and *cis* configurations as well as the ligand chemical modification, affording N,O- and N,N- plus O,O-chelation within the CPs. The substrate packing proves important in this process: no isomerization was found in the CPs for indigo (or 6,6′-dibromoindigo) with Fe adsorbed on the Ag(100) surface. DFT calculations further shed light on the molecular adsorption, coordination motifs and isomerization process. This investigation points to a fascinating playground for the realization of interfacial metal-organic nanosystems, in which tuning of the linker isomerization affords different types of coordination polymers.

Results and Discussion

Deposition of a submonolayer of indigo molecules and Fe atoms on a Ag(111) surface held at room temperature (r.t., 300 K) and subsequent annealing at 573 K leads to the formation of isolated CPs, as shown in Figure 1a. Within these CPs, one can distinguish two kinds of molecular arrangements considering the angle between the molecular axis and the CP direction. While an acute angle of approximately 73° is measured in CP–A segments (rendered

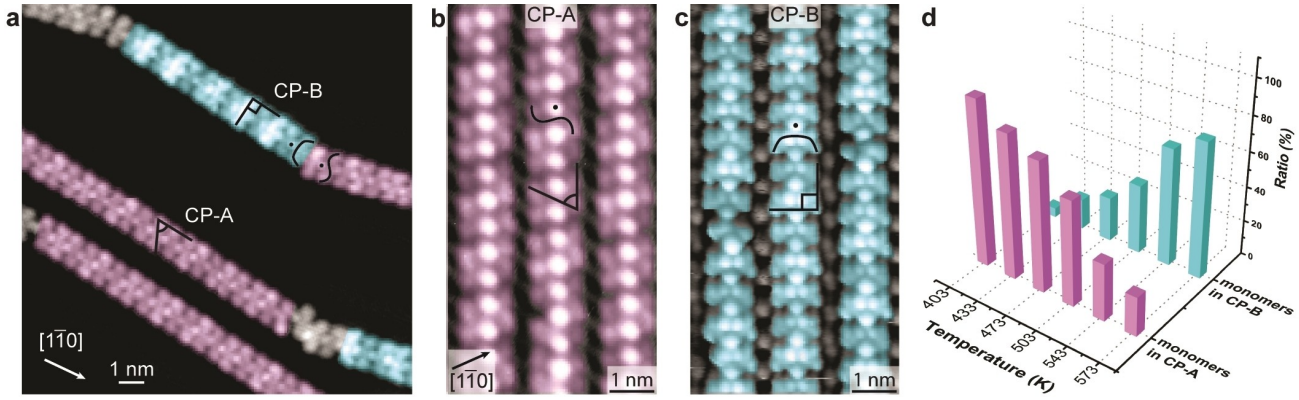

Figure 1. STM analysis of CPs formed by indigo or Tyrian purple molecules and Fe atoms on Ag(111). a) Representative overview STM image (0.1 V, 100 pA, 4.6 K) of the CPs on Ag(111) after annealing a submonolayer coverage of indigo with Fe atoms at 573 K. Two types of polymers are observed, differing in the monomer shape and the orientation of the monomer backbone with respect to the chain direction: CP–A and CP–B, coloured cyan and magenta, respectively. b-c) High-resolution STM images of CP–A (1.5 V, 70 pA, r.t.) and CP–B (1.0 V, 100 pA, r.t.) evolving on Ag(111) upon annealing a submonolayer of Tyrian purple with Fe atoms. A high symmetry direction of the Ag(111) surface as well as the angles between the molecular backbone and the chain direction are indicated. d) Distribution of monomers in CP–A and CP–B as a function of annealing temperature of Tyrian purple and Fe on Ag(111).

in a magenta colour scale), a right angle is obvious in CP–B segments (rendered in a cyan colour scale). The monomer of CP–A is imaged in the STM data as an S-shaped protrusion, attributed to the organic ligand (marked by a S-line on Figure 1a) and a bright round protrusion, attributed to the metal centre (marked by a dot on Figure 1a). Notably, the S-shaped protrusion is consistent with the STM imaging of indigo on Cu(111).[30] CP–B is comprised of a clearly distinguishable monomer: a U-shaped and a round protrusion, indicated on Figure 1a by a U-line and a dot, respectively. Interestingly, further annealing of the sample at 623 K, leads to CPs comprised predominantly of extended CP–B, which aggregate into self-assembled islands (see Figure S1).

Similar results are obtained by employing the same fabrication protocol after replacement of indigo with Tyrian purple: both CP–A and CP–B segments can be found as shown in the high-resolution images of Figure 1(b–c). These are identified by the distinctive monomer features, allowing us to conclude that the same CPs are formed by both natural compounds of indigo and Tyrian purple on Ag(111). The overview STM images shown in Figure S2 reveal that CP–B is predominantly expressed following annealing at 573 K. Figure 1d presents the relationship between annealing temperature and the portions of the monomers within CP–A and CP–B (raw data in Figure S3). Similar to the case of indigo, CP–B is clearly preferred with increasing annealing temperature.

To obtain a chemical identification of the monomers within CP–A and CP–B, a series of XPS measurements was carried out. In particular, relevant core levels were probed to investigate the chemical alterations to the monomer deposited at r.t. on Ag(111) before and after the addition of the second component (Fe) and heat treatment. The complete set of data can be found in Figure S4, whereas Figure 2 shows the most informative spectra corresponding to the O 1s and N 1s regions after initial deposition of Tyrian purple on the Ag(111) surface at r.t. (bottom), and following the addition of Fe atoms and annealing at 473 K (top). Without Fe deposition, the O 1s spectrum shows a prominent peak with a binding energy (BE) centred at 530.2 eV, which is assigned to the *keto* group in the indigo backbone hybridizing strongly with the substrate metal

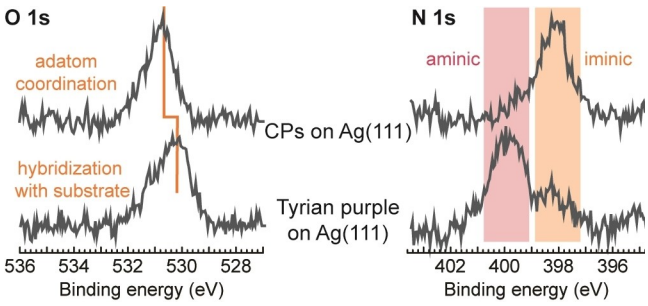

Figure 2. O 1s and N 1s spectra of pure Tyrian purple on the Ag(111) surface (bottom) and with the addition of Fe adatoms and annealing to 473 K, corresponding to the formation of CPs (top).

states.[31] A small shoulder can be noticed at 531.2 eV, which might originate from *keto* groups without strong substrate hybridization[31] presumably due to local supramolecular interactions. Correspondingly, the N 1s spectrum shows two peaks with a BE of 399.9 eV and 398.0 eV, in good accord with aminic and iminic N atoms on metal surfaces, respectively.[32] We thus infer that a small portion of N–H scission occurs already at r.t. on the Ag(111) surface. Concomitantly, we observe the scission of C–Br (cf. Br 3p spectra in Figure S4d).[33] This is in line with reports of brominated organic molecule monomers that undergo C–Br bond scission on Ag(111).[34] The activated C atom may engage in C–C homocoupling,[34a] C–Ag[34b] bonds with the native adatoms of the surface or be passivated by H atoms.[34c] On neither Ag(111) nor Ag(100), there is evidence of reactive C atoms resulting from the C–Br bond cleavage in the STM images (as e.g. dimers, oligomers or metal-organic intermediates, Figure S5). Thus, it is proposed that this C site is passivated with H[34c] originating from the on-surface N–H scission and/or from residual H_2 in the ultra-high vacuum environment.[35] Surface Br atoms are evident both in the XPS spectra (Figure S4d) and in the STM data as bright protrusions[36] between the CPs (see Figure 1b,c), where they mediate the CP self-assembly into islands by hydrogen bonding.[37] After triggering CP formation by addition of Fe atoms and annealing to 473 K, the O 1s and N 1s spectra show sole peaks centred at 530.8 eV and 398.1 eV, respectively. The O 1s shift to higher binding energy is consistent with observations of on-surface coordination between carboxylate moieties and Fe atoms.[38] Also the N 1s BE is consistent with Fe coordination.[39] Upon annealing to 673 K, these regions remain unaffected, indicating that the O and N atoms have the same chemical state in CP–A and CB–B (Figure S4a,b). We thus conclude that all N and O atoms are coordinated by Fe atoms in both CP–A and CP–B polymers.

With the chemical identification of the monomers, we turn our attention to the high resolution STM and nc-AFM imaging, in order to identify the monomers isomeric forms in CP–A and CP–B. Upon close inspection, we attribute CP–A to molecular monomers of *trans*-dehydroindigo stabilized by two kinds of coordination bonds (C=O···Fe and N···Fe), affording N,O chelation. A structural model was optimized by DFT (Figure 3b). The model clearly demonstrates the double *trans*-N,O coordination of Fe by two dehydroindigo molecules. The distance *d* between two adjacent Fe atoms is 6.33 Å, in good agreement with the measured value of 6.3 ± 0.2 Å. The assigned structure is further supported by the simulated STM appearance (Figure 3c), which closely reproduces the experimental STM image, manifesting that the two small dots near the centre of every single *trans*-dehydroindigo can be associated to the two carbonyl groups. To indisputably confirm the coordination structure, bond-resolved nc-AFM technique with CO tip functionalization[27f] was also utilized to inspect CP–A (Figure 3a, right and Figure S7). The confirmation of the *trans*-dehyroindigo configuration is achieved via the clear visualization of the indole 6-membered ring orientation and the adatom in the coordination node, in good agreement

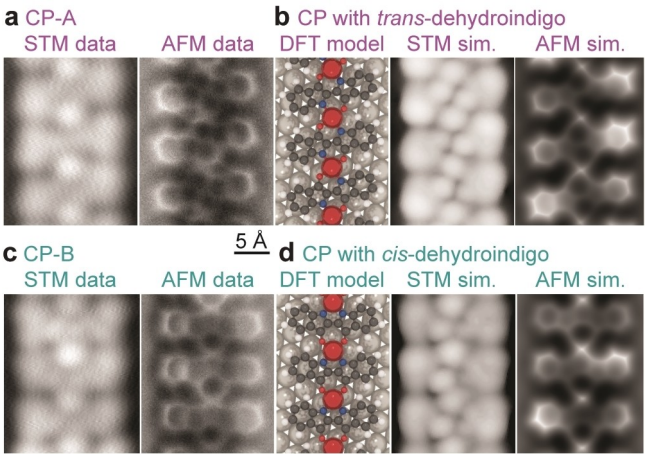

Figure 3. CP–A and CP–B structural identification. a) High resolution STM image (left, −0.1 V, 100 pA, 4.6 K) and AFM image (right) of a representative CP–A chain formed by indigo and Fe on Ag(111). b) DFT optimized model of a CP chain with three *trans*-dehydroindigo monomers next to the corresponding simulated STM image[41] (centre) and AFM image[40] (right). c) High resolution STM image (left, 0.1 V, 100 pA, 4.6 K) and AFM image (right) of a representative CP–B chain formed by indigo and Fe on Ag(111). d) DFT optimized model with three *cis*-dehydroindigo monomers next to the corresponding simulated STM image[41] (centre) and AFM image[40] (right). All images are on the same scale. C, O, N, H, Fe and Ag atoms are depicted by black, smaller red, blue, white, larger rust and silver spheres, respectively.

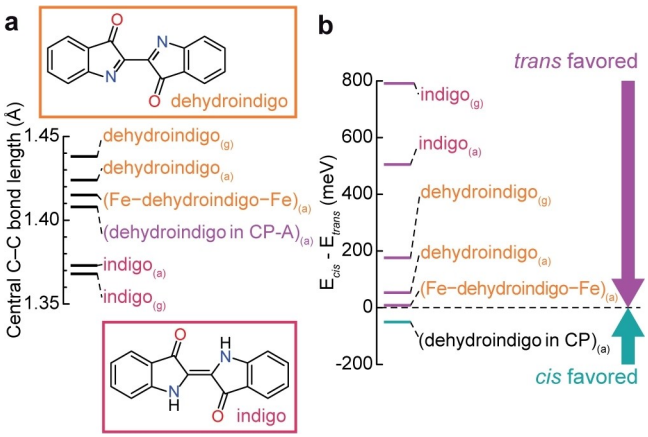

Figure 4. DFT analysis of geometry and energy of the isomerization. a) Comparison of the central C–C bond lengths of *trans* indigo and dehydroindigo in different environments, as indicated. b) Energetics of the indigo and dehydroindigo isomerization. Gas phase and Ag(111) adsorbed states are indicated by the subscripts (g) and (a), respectively.

with the AFM-simulation of the model. In addition, the images show that the bright features associated with the carbonyl groups are on opposite sides of the molecule (see also the AFM simulation[40] in Figure S8).

Likewise, we studied the CP–B that features monomers perpendicular to the chain direction, separated by the same distance *d*. To account for the symmetry of the molecular monomer, we ascribe CP–B (Figure 3c and Figure S7) to a CP composed of *cis*-dehydroindigo and obtained the DFT-optimized structural model shown in Figure 3d, left. Conceivably, an indole of the *trans*-dehydroindigo flips around the centre C–C bond, affording N,N–O,O coordination. The excellent match of the simulated STM (Figure 3d, centre) and bond-resolved AFM (Figure 3d, right) with the corresponding experimental data unambiguously verifies the proposed molecular model.

Indigo features a central C=C double bond (see inset outlined in pink, Figure 4a). The isomerization observed would require a rotation around this bond, which would be indicative of the nature of a single C–C bond. By means of DFT we investigated the central C–C bond lengths of *trans*-indigo and *trans*-dehydroindigo (see inset outlined in orange in Figure 4a) as a measure of the single vs. double bond character. Indeed, for isolated species the bond length increases significantly from the indigo molecule (1.368 Å) to dehydroindigo (1.438 Å). An increase in the bond length distance is also found for the corresponding surface adsorbed species indicating that a rotation around this bond is likely feasible due to the N–H bond scission caused by the Fe coordination. A simulation of the isomerization process for the model system of (Fe-dehydroindigo-Fe)$_{(a)}$ is shown in Supporting Information Movie S1.

Next, the propensity of the indigo type dyes towards isomerization is addressed. To unravel the related thermodynamics, extensive DFT calculations were carried out comparing the energy difference between *cis* and *trans* configuration of the molecule in different environments (Figure 4b). As expected, in the gas phase and on the surface, *trans*-indigo is favoured over *cis*-indigo for both molecules. This energy difference between the isomers decreases significantly for dehydroindigo due to the conversion of the central C=C double bond into a single bond. Moreover, for both, indigo and dehydroindigo, the surface environment decreases the energy difference between *cis* and *trans*. However, in all these cases the *trans* isomer is favoured. It is only within the coordination polymers that the *cis*-dehydroindigo is clearly favoured over *trans*-dehydroindigo, which indicates that for this chemistry both the Fe coordination and the surface environment are key elements.

Finally, to gain insights into the influence of the epitaxy on the isomerization, the substrate was changed to Ag(100). Unexpectedly, only CP–A arrangements were detected in the STM investigation, even if the sample of Tyrian purple and Fe is annealed up to 673 K (Figure S9a-e). The corresponding DFT model in Figure S9f shows that all Fe atoms are located on hollow sites and the CP periodicity matches very well the Ag(100) atomic lattice. In comparison, for CP–A on Ag(111), every third Fe atom is on a hollow site. A CP with *trans*-monomers is energetically favoured over *cis*-monomers on Ag(100) by 96 meV/monomer. Detailed analysis shows that the key factor favouring the isomerization in the CP on Ag(111) is the strain imposed by the substrate; another key factor is the stronger binding between the CP with *cis*-dehydroindigo to the substrate than the CP with *trans*-dehydroindigo on Ag(111) (see Figure S10). This is not true on Ag(100). The stronger overall

adsorption energy of dehydroindigo on Ag(100) is presumably also hindering the rotation required for the isomerization into the *cis* form. As a result, the isomerization is absent on this surface.

Based on DFT modelling and analysis, it is expected that the obtained CPs on Ag(111) are conductive, whereby the density of states in the vicinity of the Fermi level is quite similar for both isomers. Intriguingly, the DFT calculations indicate that on both Ag(111) and Ag(100) the CPs are spin-crossover systems, with spin-crossover energy barriers of ~100 meV. Notably, the ligand field that determines the splitting between Fe d states is different in the CPs with *cis*-dehydroindigo and CPs with *trans*-dehydroindigo, which aspects and their implications will be explored further in a future publication.

Conclusion

We have demonstrated that two natural dyes (indigo and Tyrian purple) are suitable to generate high-quality, extended CPs obtained in a metal-directed assembly scenario on planar silver surfaces (see pathways described in Scheme 1). CPs incorporating *trans*-dehydroindigo molecules and Fe adatoms are realized on Ag(111) and Ag(100). The dehydrogenation caused by the Fe-coordination, transforms the central double bond of the molecule into a single bond, enabling a rotation of the indole moieties on both surfaces. On Ag(111), the difference in the binding of *cis* and *trans* dehydroindigo isomers to the surface mediates an isomerization of the molecular linker within the CP. For this isomerization, both the Fe coordination and the presence of the Ag substrate are crucial: their combination results in an energy gain when the molecular monomer transforms from *trans* to *cis*. These results reveal the realization of interfacial metal-organic nanosystems, where different types of CPs are accessible by linker isomerization, offering a new pathway to alter the physicochemical properties of the respective CPs. Last but not least, with the presented strategy of employing such natural dyes, biocompatibility and biodegradability may be imparted in such advanced composites.

Supporting Information

The authors have cited additional references within the Supporting Information.[42]

Acknowledgements

We acknowledge funding of the German Research Foundation (DFG) through the priority program COORNETs (SPP1928) with project number 316890188 and through project number 453903355 (A.R.). Support and resources were provided by the PARAM Yukti, National Supercomputing Mission and TUE-CMS, both at JNCASR, Bangalore, India. H.X. thanks the China Scholarship Council (CSC) for a doctoral scholarship. B.Y. acknowledges the Collaborative Innovation Center of Suzhou Nano Science & Technology, the Suzhou Key Laboratory of Surface and Interface Intelligent Matter (Grant SZS2022011), and the 111 Project. S.N. also acknowledges the Sheikh Saqr Laboratory of ICMS, JNCASR and the Anna Boyksen Fellowship of the Technical University of Munich, Institute for Advanced Study. A.C.P. benefits from the framework of H.F.R.I. Call "Basic Research Financing (Horizontal support of all Sciences)" under the National Recovery and Resilience Plan "Greece 2.0" funded by the European Union—NextGenerationEU (H.F.R.I. Project Number: 15609). Open Access funding enabled and organized by Projekt DEAL.

Conflict of Interest

The authors declare no conflict of interest.

Data Availability Statement

The data that support the findings of this study are available from the corresponding author upon reasonable request.

Keywords: Indigo · Isomerization · Coordination Polymers · Scanning Tunneling Microscopy · Noncontact Atomic Force Microscopy

[1] N. Guyard, L. Skaltousnis, G. Eisenbrand, *Indirubin, the red shade of indigo*, Life in Progress Edition **2006**.
[2] a) D. V. Konarev, S. S. Khasanov, A. V. Kuzmin, A. F. Shestakov, A. Otsuka, H. Yamochi, G. Saito, R. N. Lyubovskaya, *Dalton Trans.* **2016**, *45*, 17095–17099; b) F. S. Guo, R. A. Layfield, *Chem. Commun.* **2017**, *53*, 3130–3133; c) D. V. Konarev, L. V. Zorina, S. S. Khasanov, A. F. Shestakov, A. M. Fatalov, A. Otsuka, H. Yamochi, H. Kitagawa, R. N. Lyubovskaya, *Inorg. Chem.* **2018**, *57*, 583–589; d) P. Mondal, A. Das, G. K. Lahiri, *Inorg. Chem.* **2016**, *55*, 1208–1218.
[3] a) D. V. Konarev, S. S. Khasanov, A. F. Shestakov, A. M. Fatalov, M. S. Batov, A. Otsuka, H. Yamochi, H. Kitagawa, R. N. Lyubovskaya, *Dalton Trans.* **2017**, *46*, 14365–14372; b) M. Chatterjee, P. Ghosh, K. Beyer, A. Paretzki, J. Fiedler, W. Kaim, G. K. Lahiri, *Chem. Asian J.* **2018**, *13*, 118–125.
[4] W. Beck, K. Sünkel, *Z. Anorg. Allg. Chem.* **2020**, *646*, 248–255.
[5] E. Vorobyeva, F. Lissel, M. Salanne, M. R. Lukatskaya, *ACS Nano* **2021**, *15*, 15422–15428.
[6] a) W. Kaim, G. K. Lahiri, *Coord. Chem. Rev.* **2019**, *393*, 1–8; b) E. D. Glowacki, G. Voss, N. S. Sariciftci, *Adv. Mater.* **2013**, *25*, 6783–6799.
[7] A. Honda, K. Noda, Y. Tamaki, K. Miyamura, *Mater.* **2016**, *9*, 837.
[8] K. M. Elsabawy, A. M. Fallatah, *Inorg. Chem. Commun.* **2018**, *92*, 78–83.
[9] S. F. Zhang, F. Xiong, Z. He, Y. Liang, J. R. Xue, L. H. Jing, D. B. Qin, *Polyhedron* **2015**, *102*, 401–409.
[10] F. Q. Wang, C. M. Wang, Z. C. Yu, K. H. Xu, X. Y. Li, Y. Y. Fu, *Polyhedron* **2016**, *105*, 49–55.
[11] Z. H. Yan, X. Y. Li, L. W. Liu, S. Q. Yu, X. P. Wang, D. Sun, *Inorg. Chem.* **2016**, *55*, 1096–1101.
[12] D. R. Talham, M. W. Meisel, *Chem. Soc. Rev.* **2011**, *40*, 3356–3365.

[13] a) D. Heim, D. Écija, K. Seufert, W. Auwärter, C. Aurisicchio, C. Fabbro, D. Bonifazi, J. V. Barth, *J. Am. Chem. Soc.* **2010**, *132*, 6783–6790; b) T. A. Pham, F. Song, M. N. Alberti, M.-T. Nguyen, N. Trapp, C. Thilgen, F. Diederich, M. Stöhr, *Chem. Commun.* **2015**, *51*, 14473–14476; c) M. Knor, H.-Y. Gao, S. Amirjalayer, A. Studer, H. Gao, S. Du, H. Fuchs, *Chem. Commun.* **2015**, *51*, 10854–10857; d) A. C. Papageorgiou, J. Li, S. C. Oh, B. Zhang, Ö. Sağlam, Y. Guo, J. Reichert, A. B. Marco, D. Cortizo-Lacalle, A. Mateo-Alonso, J. V. Barth, *Nanoscale* **2018**, *10*, 9561–9568; e) J. Liu, M. Abel, N. Lin, *J. Phys. Chem. Lett.* **2022**, *13*, 1356–1365; f) X. Yu, Q. Sun, M. Liu, W. Du, Y. Liu, L. Cai, Z. Zha, J. Pan, F. Kang, W. Gao, D. Yang, X. Qiu, W. Xu, *Chem. Mater.* **2022**, *34*, 1770–1777; g) L. Song, B. Yang, F. Liu, K. Niu, Y. Han, J. Wang, Y. Zheng, H. Zhang, Q. Li, L. Chi, *J. Phys. Chem. C* **2020**, *124*, 12390–12396.

[14] a) V. M. Santhini, C. Wäckerlin, A. Cahlík, M. Ondráček, S. Pascal, A. Matěj, O. Stetsovych, P. Mutombo, P. Lazar, O. Siri, P. Jelínek, *Angew. Chem. Int. Ed.* **2021**, *60*, 439–445; b) F. Frezza, F. Schiller, A. Cahlík, J. E. Ortega, J. V. Barth, A. Arnau, M. Blanco-Rey, P. Jelínek, M. Corso, I. Piquero-Zulaica, *Nanoscale* **2023**, *15*, 2285–2291.

[15] a) J. Liu, Y. Gao, T. Wang, Q. Xue, M. Hua, Y. Wang, L. Huang, N. Lin, *ACS Nano* **2020**, *14*, 11283–11293; b) B. Mallada, P. Błoński, R. Langer, P. Jelínek, M. Otyepka, B. de la Torre, *ACS Appl. Mater. Interfaces* **2021**, *13*, 32393–32401; c) C. Wäckerlin, A. Cahlík, J. Goikoetxea, O. Stetsovych, D. Medvedeva, J. Redondo, M. Švec, B. Delley, M. Ondráček, A. Pinar, M. Blanco-Rey, J. Kolorenč, A. Arnau, P. Jelínek, *ACS Nano* **2022**, *16*, 16402–16413.

[16] C. Miliani, A. Romani, G. Favaro, *Spectrochim. Acta Part A* **1998**, *54*, 581–588.

[17] a) S. Yamazaki, A. L. Sobolewski, W. Domcke, *Phys. Chem. Chem. Phys.* **2011**, *13*, 1618–1628; b) J. Weinstein, G. M. Wyman, *J. Am. Chem. Soc.* **1956**, *78*, 4007–4010; c) J. S. S. de Melo, R. Rondao, H. D. Burrows, M. J. Melo, S. Navaratnam, R. Edge, G. Voss, *ChemPhysChem* **2006**, *7*, 2303–2311; d) G. M. Wyman, *Chem. Rev.* **1955**, *55*, 625–657; e) C. R. Giuliano, L. D. Hess, J. D. Margerum, *J. Am. Chem. Soc.* **1968**, *90*, 587–594.

[18] a) W. R. Brode, E. G. Pearson, G. M. Wyman, *J. Am. Chem. Soc.* **1954**, *76*, 1034–1036; b) M. Moreno, J. M. Ortiz-Sanchez, R. Gelabert, J. M. Lluch, *Phys. Chem. Chem. Phys.* **2013**, *15*, 20236–20246; c) M. R. Haggmark, G. Gate, S. Boldissar, J. Berenbeim, A. L. Sobolewski, M. S. de Vries, *Chem. Phys.* **2018**, *515*, 535–542; d) J. Pina, D. Sarmento, M. Accoto, P. L. Gentili, L. Vaccaro, A. Galvao, J. S. S. de Melo, *J. Phys. Chem. B* **2017**, *121*, 2308–2318.

[19] a) D. C. Nobre, C. Cunha, A. Porciello, F. Valentini, A. Marrocchi, L. Vaccaro, A. M. Galvao, J. S. S. de Melo, *Dyes Pigm.* **2020**, *176*, 108197; b) Š. Budzák, J. Jovaišaitė, C.-Y. Huang, P. Baronas, K. Tulaitė, S. Juršėnas, D. Jacquemin, S. Hecht, *Chem. Eur. J.* **2022**, *28*, e202200496.

[20] a) J. Setsune, H. Wakemoto, K. Matsukawa, S. Ishihara, R. Yamamoto, T. Kitao, *J. Chem. Soc. Chem. Commun.* **1982**, 1022–1023; b) Y. Sueishi, K. Ohtani, N. Nishimura, *Bull. Chem. Soc. Jpn.* **1985**, *58*, 810–814.

[21] G. Miehe, P. Susse, V. Kupcik, E. Egert, M. Nieger, G. Kunz, R. Gerke, B. Knieriem, M. Niemeyer, W. Luttke, *Angew. Chem. Int. Ed.* **1991**, *30*, 964–967.

[22] D. Farka, M. Scharber, E. D. Glowacki, N. S. Sariciftci, *J. Phys. Chem. A* **2015**, *119*, 3563–3568.

[23] a) C. Y. Huang, A. Bonasera, L. Hristov, Y. Garmshausen, B. M. Schmidt, D. Jacquemin, S. Hecht, *J. Am. Chem. Soc.* **2017**, *139*, 15205–15211; b) C. Petermayer, H. Dube, *Acc. Chem. Res.* **2018**, *51*, 1153–1163.

[24] G. Haucke, G. Graness, *Angew. Chem. Int. Ed.* **1995**, *34*, 67–68.

[25] M. U. Munshi, J. Martens, G. Berden, J. Oomens, *J. Phys. Chem. A* **2019**, *123*, 8226–8233.

[26] M. A. M. El-Mansy, I. S. Yahia, S. Alfaify, *Org. Opto-Elect.* **2015**, *1*, 39–45.

[27] a) P. A. Held, H. Fuchs, A. Studer, *Chem. Eur. J.* **2017**, *23*, 5874–5892; b) Q. Shen, H. Y. Gao, H. Fuchs, *Nano Today* **2017**, *13*, 77–96; c) L. Grill, S. Hecht, *Nat. Chem.* **2020**, *12*, 115–130; d) F. Klappenberger, Y. Q. Zhang, J. Bjork, S. Klyatskaya, M. Ruben, J. V. Barth, *Acc. Chem. Res.* **2015**, *48*, 2140–2150; e) J. V. Barth, G. Costantini, K. Kern, *Nature* **2005**, *437*, 671–679; f) L. Gross, F. Mohn, N. Moll, P. Liljeroth, G. Meyer, *Science* **2009**, *325*, 1110–1114.

[28] a) D. Skomski, C. D. Tempas, G. S. Bukowski, K. A. Smith, S. L. Tait, *J. Chem. Phys.* **2015**, *142*, 101913; b) M. Koudia, E. Nardi, O. Siri, M. Abel, *Nano Res.* **2017**, *10*, 933–940.

[29] a) N. Lin, S. Stepanow, M. Ruben, J. V. Barth, *Top. Curr. Chem.* **2009**, *287*, 1–44; b) J. V. Barth, *Surf. Sci.* **2009**, *603*, 1533–1541; c) S. Stepanow, N. Lin, J. V. Barth, *J. Phys. Condens. Matter* **2008**, *20*, 184002; d) L. Dong, Z. A. Gao, N. Lin, *Prog. Surf. Sci.* **2016**, *91*, 101–135.

[30] a) C. J. Villagómez, F. Buendía, L. O. Paz-Borbón, B. Fuentes, T. Zambelli, X. Bouju, *J. Phys. Chem. C* **2022**, *126*, 14103–14115; b) C. J. Villagomez, O. Guillermet, S. Goudeau, F. Ample, H. Xu, C. Coudret, X. Bouju, T. Zambelli, S. Gauthier, *J. Chem. Phys.* **2010**, *132*, 074705.

[31] L. Jiang, A. C. Papageorgiou, S. C. Oh, Ö. Sağlam, J. Reichert, D. A. Duncan, Y.-Q. Zhang, F. Klappenberger, Y. Guo, F. Allegretti, S. More, R. Bhosale, A. Mateo-Alonso, J. V. Barth, *ACS Nano* **2016**, *10*, 1033–1041.

[32] a) A. C. Papageorgiou, K. Diller, S. Fischer, F. Allegretti, F. Klappenberger, S. C. Oh, Ö. Sağlam, J. Reichert, A. Wiengarten, K. Seufert, W. Auwärter, J. V. Barth, *J. Phys. Chem. C* **2016**, *120*, 8751–8758; b) Q. Li, B. Yang, J. Björk, Q. Zhong, H. Ju, J. Zhang, N. Cao, Z. Shi, H. Zhang, D. Ebeling, A. Schirmeisen, J. Zhu, L. Chi, *J. Am. Chem. Soc.* **2018**, *140*, 6076–6082.

[33] T. Wang, H. F. Lv, L. Feng, Z. J. Tao, J. M. Huang, Q. T. Fan, X. J. Wu, J. F. Zhu, *J. Phys. Chem. C* **2018**, *122*, 14537–14545.

[34] a) L. Wang, R. Zhu, Z. Shen, Y. Song, L. She, X. Wang, Y. Jia, Z. Zhang, W. Zhang, *J. Am. Chem. Soc.* **2023**, *145*, 1660–1667; b) L. Grossmann, D. A. Duncan, S. P. Jarvis, R. G. Jones, S. De, J. Rosen, M. Schmittel, W. M. Heckl, J. Björk, M. Lackinger, *Nanoscale Horiz.* **2022**, *7*, 51–62; c) J. Liu, Q. W. Chen, K. Cai, J. Li, Y. R. Li, X. Yang, Y. J. Zhang, Y. F. Wang, H. Tang, D. H. Zhao, K. Wu, *Nat. Commun.* **2019**, *10*, 2545.

[35] A. Sánchez-Grande, J. I. Urgel, A. Cahlík, J. Santos, S. Edalatmanesh, E. Rodríguez-Sánchez, K. Lauwaet, P. Mutombo, D. Nachtigallová, R. Nieman, H. Lischka, B. de la Torre, R. Miranda, O. Gröning, N. Martín, P. Jelínek, D. Écija, *Angew. Chem. Int. Ed.* **2020**, *59*, 17594–17599.

[36] J. Liu, Q. Chen, Q. He, Y. Zhang, X. Fu, Y. Wang, D. Zhao, W. Chen, G. Q. Xu, K. Wu, *Phys. Chem. Chem. Phys.* **2018**, *20*, 11081–11088.

[37] J. Lu, D.-L. Bao, H. Dong, K. Qian, S. Zhang, J. Liu, Y. Zhang, X. Lin, S.-X. Du, W. Hu, H.-J. Gao, *J. Phys. Chem. Lett.* **2017**, *8*, 326–331.

[38] S. L. Tait, Y. Wang, G. Costantini, N. Lin, A. Baraldi, F. Esch, L. Petaccia, S. Lizzit, K. Kern, *J. Am. Chem. Soc.* **2008**, *130*, 2108–2113.

[39] J. M. Gottfried, K. Flechtner, A. Kretschmann, T. Lukasczyk, H. P. Steinruck, *J. Am. Chem. Soc.* **2006**, *128*, 5644–5645.

[40] a) P. Hapala, G. Kichin, C. Wagner, F. S. Tautz, R. Temirov, P. Jelínek, *Phys. Rev. B* **2014**, *90*, 085421; b) P. Hapala, R.

Temirov, F. S. Tautz, P. Jelínek, *Phys. Rev. Lett.* **2014**, *113*, 226101.
[41] J. Tersoff, D. R. Hamann, *Phys. Rev. B* **1985**, *31*, 805–813.
[42] a) I. Horcas, R. Fernández, J. M. Gómez-Rodríguez, J. Colchero, J. Gómez-Herrero, A. M. Baro, *Rev. Sci. Instrum.* **2007**, *78*, 013705; b) A. Riss, *J. Open Source Software* **2022**, *7*, 4644; c) P. Giannozzi, S. Baroni, N. Bonini, M. Calandra, R. Car, C. Cavazzoni, D. Ceresoli, G. L. Chiarotti, M. Cococcioni, I. Dabo, A. Dal Corso, S. de Gironcoli, S. Fabris, G. Fratesi, R. Gebauer, U. Gerstmann, C. Gougoussis, A. Kokalj, M. Lazzeri, L. Martin-Samos, N. Marzari, F. Mauri, R. Mazzarello, S. Paolini, A. Pasquarello, L. Paulatto, C. Sbraccia, S. Scandolo, G. Sclauzero, A. P. Seitsonen, A. Smogunov, P. Umari, R. M. Wentzcovitch, *J. Phys. Condens. Matter* **2009**, *21*, 395502; d) I. Hamada, *Phys. Rev. B* **2014**, *89*, 121103; e) K. Lee, É. D. Murray, L. Kong, B. I. Lundqvist, D. C. Langreth, *Phys. Rev. B* **2010**, *82*, 081101; f) P. E. Blöchl, O. Jepsen, O. K. Andersen, *Phys. Rev. B* **1994**, *49*, 16223–16233.

Manuscript received: December 12, 2023
Accepted manuscript online: January 18, 2024
Version of record online: February 14, 2024